



Combined 3D-QSAR modeling and molecular docking study on 1,4-dihydroindeno[1,2-c]pyrazoles as VEGFR-2 kinase inhibitors

Huahui Zeng, Huabei Zhang*

Key Laboratory of radiopharmaceuticals of Ministry of Education, College of Chemistry, Beijing Normal University, Beijing, 100875, China

ARTICLE INFO

Article history:

Received 20 October 2009

Received in revised form 5 March 2010

Accepted 18 April 2010

Available online 24 April 2010

Keywords:

VEGFR-2

1,4-dihydroindeno[1,2-c]pyrazoles

3D-QSAR

CoMFA

CoMSIA

Molecular docking

ABSTRACT

The vascular endothelial growth factor (VEGF) and its receptor tyrosine kinases VEGFR-2 are attractive targets for the development of novel anticancer agents. To understand the structure–activity correlation of 1,4-dihydroindeno[1,2-c]pyrazole-based VEGFR-2 inhibitors, we have carried out a combined molecular docking and three-dimensional quantitative structure–activity relationship (3D-QSAR) modeling study. The study has resulted in two types of satisfactory substructure-based 3D-QSAR models, including the CoMFA model (r^2 , 0.931; q^2 , 0.600) and CoMSIA model (r^2 , 0.928; q^2 , 0.569), for predicting the biological activity of new compounds. The detailed microscopic structures of VEGFR-2 binding with inhibitors have been studied by molecular docking. We have also developed docking based 3D-QSAR models (CoMFA with r^2 , 0.958; q^2 , 0.563; CoMSIA with r^2 , 0.965; q^2 , 0.567). The contour maps obtained from the 3D-QSAR models in combination with the docked binding structures help to better interpret the structure–activity relationship. All of the structural insights obtained from both the 3D-QSAR contour maps and molecular docking are consistent with the available experimental activity data. The satisfactory results strongly suggest that the developed 3D-QSAR models and the obtained VEGFR-2 inhibitor binding structures are reasonable for the prediction of the activity of new inhibitors and in future drug design.

© 2010 Elsevier Inc. All rights reserved.

1. Introduction

Protein kinases are characterized by their ability to transfer the γ -phosphate group of ATP to hydroxyl groups on their target proteins [1]. Among 518 protein kinases, about 90 protein kinases selectively catalyze the phosphorylation of tyrosine hydroxyl groups, and 58 of those protein tyrosine kinases were categorized as receptor tyrosine kinases (RTKs) due to the presence of a transmembrane spanning domain [2]. Further differentiation of the RTKs was achieved through comparison of their extracellular domains [3,4]. RTKs allosterically transmit extracellular signals through the plasma membrane and activate downstream signaling cascades which mediate growth, differentiation, and developmental signals in cells. Members of the Platelet-derived growth factor receptors PDGF (PDGFR- α , PDGFR- β , FLT3, CSF1R, and cKit) and vascular endothelial growth factor receptors VEGF (VEGFR-1/FLT1, VEGFR-2/KDR, and VEGFR-3/FLT4) RTK subfamilies appear to play essential roles in all stages of tumor angiogenesis, are able to form autocrine loops which mediate cancer cell growth and survival, and drive hematologic malignancies [5,6].

VEGFR-2 mediated signalling induces a series of endothelial responses such as proliferation, migration and survival and ultimately leads to new vessel formation and maturation [7]. However, abnormal regulation of angiogenesis has been found to be involved in the pathogenesis of several disorders including inflammation [8], rheumatoid arthritis [9], ocular neovascularization [10], psoriasis [11], tumor growth [12] and metastasis [13]. VEGFR-2 is internalized following phosphorylation initiated upon VEGF binding [14,15], through a clathrin-dependent mechanism [16], which triggers effective downstream cell proliferation signaling pathways and leads to tumor vascularization [17,18]. The function of nuclear VEGFR-2 is unknown at this time, and it remains to be demonstrated if gene transcription of downstream targets requires the nuclear localization of VEGFR-2 [7]. The blockage of VEGFR-2 signaling by small molecule inhibitors to the VEGFR-2 kinase domain has been shown to inhibit angiogenesis, tumor progression, and dissemination in a number of preclinical and clinical studies [19–22]. Therefore, inhibition of the VEGFR-2 has become an attractive strategy in the treatment of cancers [23].

In recent years, several successful strategies for the inhibition of angiogenesis have been effectively demonstrated in preclinical and clinical settings. Small molecule inhibitors of VEGFR-2, such as Imatinib, Gefitinib, Erlotinib, Sunitinib, Sorafenib, and Dasatinib [22], have been approved very effective for the treatment of cancers [24–30]. Up to now, there are still a lot of researches focusing on

* Corresponding author. Tel.: +86 10 58802961; fax: +86 10 58800567.

E-mail address: hbzhang@bnu.edu.cn (H. Zhang).

the development of novel inhibitors of VEGFR-2 [31–38]. Recently, a novel series of VEGFR-2 inhibitors which can selectively inhibit VEGFR-2 with high inhibitory activities has been reported by Jurgen, Dinges and coworkers [1,39–41].

In the present work, molecular modeling studies of the VEGFR-2 inhibitors [1,39–41] were performed using 3D-QSAR and docking approach. Ligand- and receptor-based 3D-QSAR approaches have been found to be valuable in further optimization and the development of novel inhibitors. Ligand-based 3D-QSAR approaches were reported to be effective for understanding the structure–activity relationships (SAR) [42]. Comparative molecular field analysis (CoMFA) [43] and comparative molecular similarity indices analysis (CoMSIA) [44] are two 3D-QSAR methods that have been successfully employed in drug design [45,46]. In CoMFA, the biological activity of molecules is correlated with their steric and electrostatic interaction energies [47]. In CoMSIA, similarity indices are calculated at regularly placed grid points for the aligned molecules. CoMSIA includes additional molecular descriptors like hydrophobic fields and hydrogen-bond donor and acceptor fields. Both 3D-QSAR methods give contour maps as output that can be used to get some general insights into the topological features of the binding site [48]. In conventional ligand-based QSAR, the active conformations are obtained through minimizing the molecules and selecting those with lower energy. While receptor-based conformation determination by docking takes into account features of the binding pocket and thus derived models are more reliable. The binding conformations of these antagonists and their alignment in the active site of the receptor were used to construct 3D-QSAR models, which can be further applied in activity prediction at a faster speed [49]. Thus the essential information gathered by performing simultaneous 3D-QSAR and molecular docking could be helpful to understand the structure–activity relationships of the series undertaken and subsequently for the design of new potent inhibitors.

2. Computational details

2.1. Data sets and alignment

Series of potent VEGFR-2 inhibitor derivatives reported by Jurgen, Dinges and coworkers [1,39–41] were chosen in this study. Of the 140 compounds reported, 112 compounds were used as a training set and the remaining 28 compounds were used as a test set, based on a random selection. The compounds in the training set were employed to build 3D-QSAR models, and those in the test set were used to evaluate the 3D-QSAR models. The compounds in the test set have a range of biological activity values similar to that of the training set. The IC_{50} values of the inhibitors were converted into pIC_{50} ($-\log IC_{50}$) and used as dependent variables in the CoMFA and CoMSIA calculations. The pIC_{50} values of the compounds studied cover an interval of about four log units. The structures of the compounds and their IC_{50} and pIC_{50} values are given in Table 1.

The 3D structures of all compounds were constructed by using molecular modeling software package Sybyl version 7.0 [50] and Geometry optimizations using the Tripos force field [51] with a distance-dependent dielectric and the Powell conjugate gradient algorithm. Gasteiger and Marsili charges were used [52]. The crystal structure of VEGFR-2 in complex with its inhibitor AAZ (PDB entry code 1Y6A, resolution: 2.10 Å) was recovered from Brookhaven Protein Database (PDB, <http://www.pdb.org/pdb/home/home.do>). After adding all the hydrogen atoms, the AAZ/1Y6A complex was relaxed 300 steps using AMBER field [51] with Kollman all-atom charges [53] for enzyme and Gasteiger and Marsili charges [52] for ligand in Sybyl. All calculations were performed on a Dell Precision 470 workstation running Redhat Linux WS 3.0 [54]. The

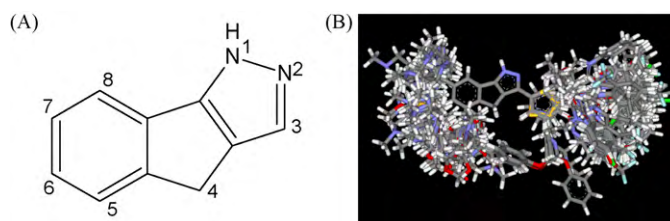


Fig. 1. Superposition of compounds in the training and test sets using the common substructure-based alignment rules. (A) Common substructure-based alignment rules; (B) superposition of compounds in the training and test sets.

most active compound 76 was used as a template for superimposition, assuming that its conformation represents the most bioactive conformation at receptor active site level. The common fragment shown in Fig. 1A was selected for Database Alignment method in SYBYL and the rest of the molecules in the data set were aligned on it (Fig. 1B).

2.2. 3D-QSAR studies

To construct good predictive QSAR models and to evaluate the contributions of electrostatic, steric, and hydrophobic effects to the activities of VEGFR-2 inhibitors, CoMFA and CoMSIA analyses were performed upon the binding conformations and their alignments derived from docking calculation.

The aligned training set molecules were placed in a 3D grid box of 2.0 Å such that the entire set was included in it. CoMFA fields were generated using sp^3 carbon probe atom carrying +1 charge to generate steric (Lennard–Jones 6–12 potential) and electrostatic fields (Coulomb potential) at each grid point [55]. The steric and electrostatic energy values in CoMFA were truncated at 30 kcal/mol. The CoMFA fields were scaled by the CoFASTD method in SYBYL7.0. The CoMSIA method defines explicit hydrophobic and hydrogen-bond donor, and acceptor descriptors in addition to the steric and electrostatic fields used in CoMFA. The same grids constructed for the CoMFA fields calculation were used for CoMSIA fields calculation. A sp^3 carbon probe atom with a charge of +1.0, a radius of 1.0 Å, hydrophobicity +1.0, and H-bond donor and acceptor property +1 was used to calculate the respective fields. The minimum-sigma was set to 2.0 kcal/mol. CoMSIA similarity indices (AF) for a molecule j with atoms i at a grid point q are calculated by the following equation:

$$A_{F,k}^q(j) = - \sum \omega_{\text{probe},k} \omega_{ik} e^{-\alpha r_{iq}^2}$$

where k represents the steric, electrostatic, hydrophobic, or hydrogen-bond donor or acceptor descriptor. The default value of 0.3 was used as the attenuation factor. A Gaussian-type distance dependence was used between the grid point q and each atom i of the molecule.

The CoMFA/CoMSIA fields combined with observed biological activities (pIC_{50}) were included in a molecular spreadsheet and partial least square (PLS) [56] methods were applied to generate 3D-QSAR models. The PLS algorithm with the leave one out (LOO) [57] cross-validation method was employed to choose optimum number of components and assess the statistical significance of each model. All cross-validated PLS analyses were performed with a column filter value of 2.0 kcal/mol. The cross-validated coefficient q^2 was calculated using the equation:

$$q^2 = 1 - \frac{\sum (Y_{\text{pred}} - Y_{\text{actu}})^2}{\sum (Y_{\text{actu}} - Y_{\text{mean}})^2}$$

where Y_{pred} , Y_{actu} , and Y_{mean} are predicted, actual, and mean values of the target property (pIC_{50}), respectively. The optimum num-

ber of components was chosen, which gave less standard error of prediction and high q^2 . And:

$$\sum (Y_{actu} - Y_{mean})^2 = PRESS$$

PRESS is the sum of squared deviations between the actual and the predicted activities of the test set molecules. In addition, the number of components, the conventional correlation coefficient (r^2), and its standard error were also computed for each model. The conventional correlation coefficient r^2 was also computed as well as the conventional correlation coefficient for the prediction of compounds in the test set r^2_{pred} . Validation is a crucial aspect of QSAR modeling. Further tests on external validation are required which was calculated using the equation [58]:

$$r^2_{m(test)} = r^2 \times \left(1 - \sqrt{r^2 - r^2_0}\right)$$

The parameters r^2 and r^2_0 are squared correlation coefficient values between observed and predicted values (or predicted versus observed values) of the test set compounds with and without intercept, respectively. The CoMFA/CoMSIA results were graphically interpreted by field contribution maps using the “STDEV*COEFF” field type.

2.3. Molecular docking

Automated docking was used to locate the appropriate binding orientations and conformations of 1,4-dihydroindeno[1,2-c]pyrazoles derivatives into the VEGFR-2 binding pocket. The powerful genetic algorithm method implemented in the program AutoDock4.0 [59] was employed. All water molecules and its ligand were removed from the original Protein Data Bank file. Polar hydrogen atoms were added and Kollman charges [53], atomic sol-

Table 1
Molecular structures of compounds and their VEGFR-2 inhibitory activity.

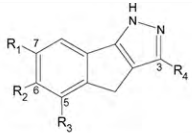
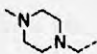
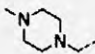
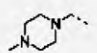
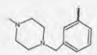
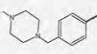
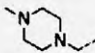
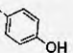
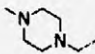
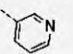
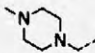
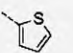
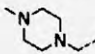
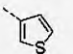
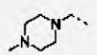
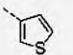
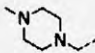
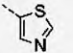
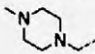
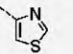
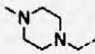
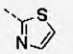
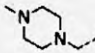
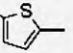
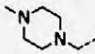
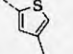
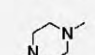
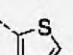
						
Compd.	R ₁	R ₂	R ₃	R ₄	IC ₅₀ (μM)	pIC ₅₀
1	H	H	H	Ph-	1.20	5.92
2	H	H		Ph-	14.10	4.85
3	H		H	Ph-	0.70	6.15
4*		H	H	Ph-	0.60	6.22
5	H	H	H		3.40	5.47
6	H	H	H		1.40	5.85
7	H		H		0.50	6.30
8	H		H		9.20	5.04
9*	H		H		1.05	5.98
10	H		H		0.40	6.40
11		H	H		0.18	6.74
12	H		H		2.84	5.55
13	H		H		7.48	5.13
14*	H		H		16.64	4.78
15	H		H		5.47	5.26
16	H		H		12.54	4.90
17	H		H		1.005	6.00

Table 1 (Continued)

18		H	H		0.143	6.84
19*		H	H		0.824	6.08
20		H	H		0.190	6.72
21		H	H		4.081	5.39
22		H	H		0.665	6.18
23		H	H		0.190	6.72
24*		H	H		0.108	6.97
25		H	H		0.147	6.83
26	H		H		0.061	7.21
27	H		H		0.180	6.74
28		H	H		0.048	7.32
29*		H	H		0.102	6.99
30	H		H		12.285	4.91
31	H		H		2.777	5.56
32	H		H		0.212	6.67
33	H		H		22.795	4.64
34*	H		H		24.158	4.62
35	H		H		0.042	7.38
36	H		H		0.459	6.34
37	H	H			7.04	5.15

vation parameters and fragmental volumes were assigned to the protein using AutoDock Tools (ADT). For validation of the docking protocol, AAZ coordinates in the crystal complex were removed and the bond orders were checked. For docking calculations, Gasteiger partial charges [52] were assigned to the 1,4-dihydroindeno[1,2-c]pyrazoles derivatives and AAZ, and non-polar hydrogen atoms were merged. All torsions were allowed to rotate during docking.

The auxiliary program AutoGrid generated the grid maps. Each grid was centered at the crystal structure of the corresponding inhibitors. The grid dimensions were $45 \times 45 \times 45 \text{ \AA}^3$ with points separated by 0.375 \AA . Lennard-Jones parameters 12-10 and 12-6, supplied with the program, were used for modeling H-bonds and van der Waals interactions, respectively. The distance-dependent dielectric permittivity of Mehler and Solmajer [60] was used for

calculation of the electrostatic grid maps. For all ligands, random starting positions, random orientations and torsions were used. The translation, quaternion and torsion steps were taken from default values in AutoDock. The Lamarckian genetic algorithm and the pseudo-Solis and Wets methods were applied for minimization using default parameters. The number of docking runs was 50. The population in the genetic algorithm was 50, the energy evaluations were 250 000 and the maximum number of iterations 27 000. After docking, the 50 solutions were clustered into groups with RMS deviations lower than 1.0 \AA . The clusters were ranked by the lowest energy representative of each cluster.

The complexes of 1,4-dihydroindeno[1,2-c]pyrazoles derivatives with VEGFR-2 resulting from molecular docking were further structurally optimized modifying the atom type and adding Gasteiger-Hückel partial charges.

3. Results and discussion

3.1. 3D-QSAR models

CoMFA and CoMSIA 3D-QSAR models were derived using a series of VEGFR-2 inhibitors, possessing receptor antagonistic activity. The chemical structures of the molecules and their actual pIC_{50} values are shown in Table 1. The data set was divided into a training set of 112 and a test set of 28 molecules. The most active compound 76 was used as a template for superimposition. The common fragment shown in Fig. 1A was selected for Database Alignment method in SYBYL and the rest of the molecules were

aligned on it. The aligned compounds were shown in Fig. 1B. The statistical parameters obtained from CoMFA and CoMSIA analysis were listed in Table 2. The best predictions were obtained by the CoMFA standard model ($q^2 = 0.600$, $r^2 = 0.884$) and CoMSIA combined steric, electrostatic and hydrophobic fields ($q^2 = 0.569$, $r^2 = 0.942$) which indicated that the built 3D-QSAR models were reliable and able to predict binding affinities of new derivatives accurately.

In CoMFA, PLS analysis of VEGFR-2 inhibitors of training set showed cross-validated q^2 of 0.600 using six principal components and non cross-validated r^2 value of 0.884; the F value and standard error are 133.692 and 0.320, respectively; the steric and electro-

Table 1 (Continued)

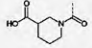
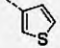
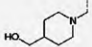
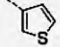
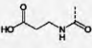
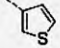
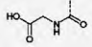
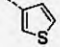
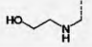
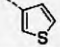
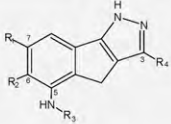
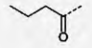
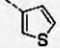
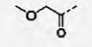
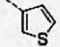
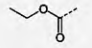
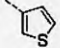
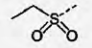
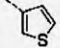
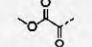
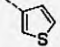
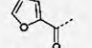
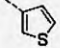
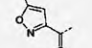
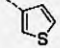
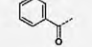
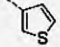
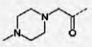
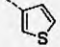
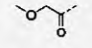
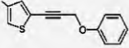
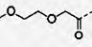
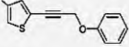
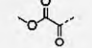
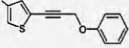
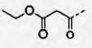
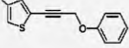
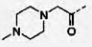
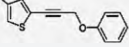
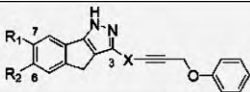
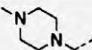
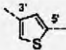
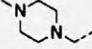
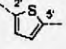
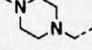
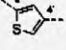
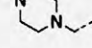
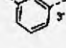
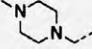
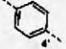
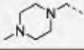
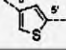
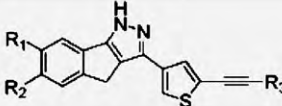
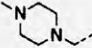
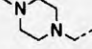
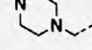
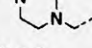
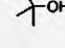
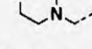
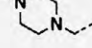
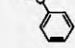
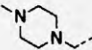
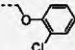
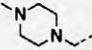
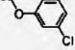
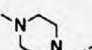
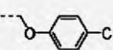
38	H	H			4.84	5.32
39*	H	H			27.89	4.55
40	H	H			0.58	6.24
41	H	H			0.41	6.39
42	H	H			0.44	6.36
						
Compd.	R ₁	R ₂	R ₃	R ₄	IC ₅₀ (uM)	pIC ₅₀
43	H	H			0.56	6.25
44*	H	H			0.07	7.15
45	H	H			0.65	6.19
46	H	H			0.31	6.51
47	H	H			0.05	7.3
48	H	H			0.11	6.96
49*	H	H			0.06	7.22
50	H	H			0.10	7.00
51	H	H			0.92	6.04
52	H	H			0.053	7.28
53	H	H			0.270	6.57
54*	H	H			0.036	7.44
55	H	H			0.263	6.58
56	H	H			0.010	8.00

Table 1 (Continued)

						
Compd.	R ₁	R ₂	X	IC ₅₀ (uM)	pIC ₅₀	
57	H			0.006	8.22	
58	H			0.022	7.66	
59*	H			0.050	7.30	
60	H			0.108	6.97	
61	H			0.962	6.02	
62		H		0.042	7.38	
						
Compd.	R ₁	R ₂	R ₃	R ₄	IC ₅₀ (uM)	pIC ₅₀
63	H		H	H	1.000	6.00
64*	H		H	n-propyl	0.075	7.12
65	H		H	-CH ₂ CH ₂ OH	0.008	8.10
66	H		H		2.370	5.63
67	H		H	-CH ₂ OCH ₃	0.023	7.64
68	H		H		0.085	7.07
69*	H		H		0.101	7.00
70	H		H		0.036	7.44
71	H		H		0.078	7.11

static contributions were found to be 52.8% and 47.2%, respectively. Therefore, the steric field had almost same influence to the electrostatic field, indicating that the steric and electrostatic interactions of the molecules with the receptor could be two important factors for VEGFR-2 antagonistic activity. The results of CoMFA analysis were summarized in Table 2. These values indicated a reasonable statistical correlation and internal predictability of CoMFA model. Statistic parameter for external validation, $r^2_{m(test)} = 0.496$, suggested the lesser extent of deviation of the predicted activity from the observed activity values for the test set compounds. The correlation between the actual and the predicted values from the final CoMFA model are shown in Fig. 2A.

The CoMSIA method defines explicit hydrophobic, hydrogen-bond donor and acceptor descriptors in addition to steric and

electrostatic fields used in CoMFA. All compounds in training set and all the five descriptors, we derived a model with high q^2 value of 0.569 for eight components and a conventional r^2 value of 0.942. The F value and standard error were 207.781 and 0.230, respectively. The steric (S), electrostatic (E), hydrophobic (H), hydrogen-bond donor (D) and hydrogen-bond acceptor (A) field descriptor contributed 15.2%, 21.6%, 22.4%, 20.5%, 20.3%, respectively. The values of the five fields were 20.0% or so, which was the average value of whole field. Statistic parameter, $r^2_{m(test)} = 0.813$, indicated that the predicted activity coincided with the observed activity values for the test set compounds and that was a reasonable model with good external predictability. CoMSIA analysis results were also summarized in Table 2. These data indicated that a reliable CoMSIA model was successfully constructed. Predicted

activities by this model versus experimental activities of inhibitors were displayed in Fig. 2B. It can be seen clearly from Fig. 2 that the predicted pIC_{50} values obtained from CoMFA and CoMSIA models are in good agreement with the actual data. The predicted activities of all the 140 compounds for both of CoMFA and CoMSIA models were also listed in Table 3.

The 3D-QSAR models were further validated using an external test set of 28 compounds. CoMFA and CoMSIA models all gave good predictions of both the training and test set compounds. Both the CoMFA and CoMSIA models have the larger $r^2_{\text{m(test)}}$ values, 0.867 and 0.896, respectively. In both models, the deviations of the predicted pIC_{50} values from the corresponding experimental pIC_{50} values are always smaller than 1 log unit.

3.2. Mapping of CoMFA and CoMSIA models

One of the attractive features of the CoMFA and CoMSIA modeling is the visualization of the results as 3D coefficient contour plots. The contour maps were generated as scalar products of coefficients and standard deviation, associated with each CoMFA or CoMSIA column. The maps generated depict regions having scaled coefficients greater than 80% (favored) or less than 20% (disfavored). It showed regions where variations of steric, electrostatic, hydrophilic, hydrogen-bond donor or acceptor nature in the structural features of the different molecules contained in the training set lead to increases or decreases in the activity. The five fields of CoMFA and CoMSIA models for the analysis based on the alignment

Table 1 (Continued)

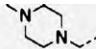
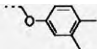
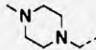
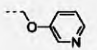
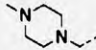
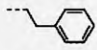
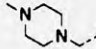
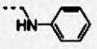
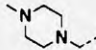
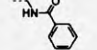
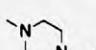
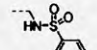
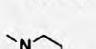
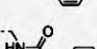
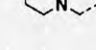
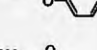
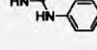
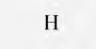
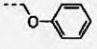
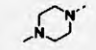
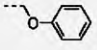
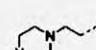
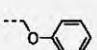
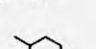

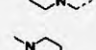
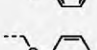
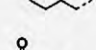

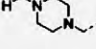
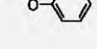
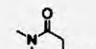
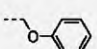
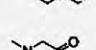
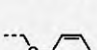
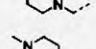

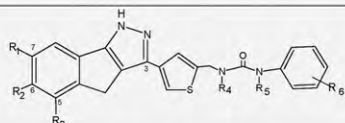
72	H		H		0.033	7.48
73	H		H		0.054	7.27
74*	H		H		0.048	7.32
75	H		H		0.036	7.44
76	H		H		0.003	8.52
77	H		H		0.045	7.35
78	H		H		0.038	7.42
79*	H		H		0.011	7.96
80	H	H	H		4.680	5.33
81	H		H		0.011	7.96
82	H		H		0.005	8.30
83	H		H		0.069	7.16
84*	H		H		0.011	7.96
85	H		H		0.009	8.05
86	H		H		0.011	7.96
87	H		H		0.007	8.15
88	H		H		0.044	7.36
89*	H		H		0.024	7.62
90	H		H		0.040	7.40

Table 1 (Continued)

91	H		H		0.042	7.38
92	H		H		0.195	6.71
93	H		H		0.020	7.70
94*	H		H		0.124	6.91
95	H		H		0.062	7.21
96	H		H		0.084	7.08
97	H		H		7.960	5.10
98	H		H		0.053	7.28
99*		H	H		0.030	7.52
100	H		H		0.048	7.32
101		H	H		0.005	8.30



Compd.	R ₁	R ₂	R ₃	R ₄	R ₅	R ₆	IC ₅₀ (uM)	pIC ₅₀
102	H		H	H	H	3-Me	0.061	7.21
103	H		H	Me	H	3-Me	0.159	6.80
104*		H	H	H	H	3-Me	0.048	7.32
105		H	H	Me	H	3-Me	0.051	7.29
106	H		H	H	H	2-Me	0.444	6.35
107	H		H	H	H	4-Me	0.308	6.51
108	H		H	H	H	2-CF ₃	2.882	5.54

of the conformations of compound 76 were presented as contour plots in Fig. 3. The colored polyhedra in the map surrounded all lattice points where the QSAR strongly associated changes in the compounds' field values with changes in biological potency.

The CoMFA contour plots show green-colored regions where increased steric is associated with enhanced activity and yellow-colored regions where increased steric bulk is associated with decreased activity (Fig. 3A). Two green polyhedrons beside the 6-, 7-position and around the terminal phenyl ring linked the imide may suggest that more bulky substituents in these areas will significantly increase the biological activities. Several big regions of yellow contour near the 5-position and the alkyne substitution suggest that more bulky substituents in these areas will significantly decrease the biological activities.

The regions where increased positive-charge is favorable for antagonist activity are indicated in blue, while regions where increased negative charge is favorable for antagonist activity are indicated in red (Fig. 3B). Two big regions of blue contours around 5-, 6-, 7-position and the imide substituent indicate that positively charged substituents may increase the antagonist activity. Several red contours near 4'-methylpiperazine group and some small red contours around the alkyne substitution suggest that more negatively charged substituents in the position will significantly improve the biological activities.

The CoMSIA contour plots show yellow-colored regions where increased hydrophobic interaction is associated with enhanced activity and white-colored regions where decreased hydrophilic interaction is associated with increased activity. As shown in Fig. 3C,

three regions of yellow contour around the alkyne substituent, the terminal phenyl ring, and the 4'-methylpiperazine group, respectively, indicate that adding hydrophobic substituents may increase the antagonist activity. However, two big white-colored polyhedrons at the imide substituent and close-by 5-, 7-position illustrate that adding hydrophobic group at this position would be detrimental to antagonist activity.

The regions where hydrogen-bond donor substituents are favorable (unfavorable) for antagonist activity are indicated in cyan (purple); The regions where hydrogen-bond acceptor substituents are favorable (unfavorable) for antagonist activity are indicated in magenta (red) (Fig. 3D). A big region of cyan contour near the amido of the imide substitution indicates that hydrogen-bond donor sub-

stituents may increase the antagonist activity. Two purple contours beside the thiophene substituent suggest hydrogen-bond donor substituents in the position will be unfavorable for antagonist activity. Several magenta contours around 4'-methylpiperazine substitution and near the carbonyl of the imide substitution indicate that hydrogen-bond acceptor substituents are favorable for the antagonist activity. A red contour around the alkyne substitution suggests that hydrogen-bond acceptor substituents in the position will decrease the biological activities.

As above, the research with CoMFA and CoMSIA basing on the ligands indicates that inhibitors with properly bigger bulky, electronegative, powerfully hydrophobic, and hydrogen-bond acceptor substituents on the 5-, 6-, 7- of framework, with small bulky,

Table 1 (Continued)

109*	H		H	H	H	3-CF ₃	0.034	7.47
110	H		H	H	H	4-CF ₃	0.281	6.55
111	H		H	H	H	2-Cl	0.199	6.70
112	H		H	H	H	3,5-di-Me	0.063	7.20
113	H		H	H	H	3,5-di-Cl	0.079	7.10
114*	H		H	Me	H	3-Me	0.159	6.80
115	H		H	H	Me	3-Me	4.807	5.32
116	H		H	Me	Me	3-Me	7.458	5.13
117	H		H	Me	H	2-Me	0.122	6.91
118	H		H	Me	H	2-Cl	0.180	6.74
119*	H		H	Me	H	3-F, 5-CF ₃	0.020	7.70
120	H		H	Me	H	3-O CF ₃	0.027	7.57
121	H		H	Et	H	3-Me	0.045	7.35
122	H		H	n-Pr	H	3-Me	0.035	7.46
123	H		H	i-Pr	H	3-Me	0.123	6.91
124*	H		H	c-Pr	H	3-Me	0.021	7.68
125	H		H	i-Bu	H	3-Me	0.164	6.79
126	H		H	i-Amyl	H	3-Me	0.262	6.58
127	H		H	CH ₃ O-	H	3-Me	0.259	6.59
128	H		H	CH ₃ OCH ₂ CH ₂	H	3-Me	0.171	6.77
129*		H	H	H	H	H	0.184	6.74
130		H	H	H	H	2-Me	0.159	6.80

Table 1 (Continued)

131		H	H	H	H	3-Me	0.048	7.32
132		H	H	H	H	4-Me	0.104	6.98
133		H	H	Me	H	3-Me	0.051	7.29
134*		H	H	Me	H	3-CF ₃	0.011	7.96
135		H	H	Me	H	3-Cl	0.012	7.92
136		H	H	Me	H	4-F	0.016	7.80
137		H	H	Me	H	4-OCF ₃	0.017	7.77
138		H	H	Me	H	3,4-di-Cl	0.018	7.74
139*		H	H	Me	H	4-Br	0.019	7.72
140		H	H	Me	H	4-Cl	0.021	7.68

Table 2

Statistical parameters of CoMFA and CoMSIA models of the training sets.

	ONC	q^2	r^2	SEE	F	r^2_{pred}	$r^2_{\text{m(test)}}$	Field contribution				
								S	E	H	D	A
CoMFA	6	0.600	0.884	0.320	133.692	0.867	0.496	0.528	0.472			
CoMSIA	8	0.569	0.942	0.230	207.781	0.896	0.813	0.152	0.216	0.224	0.205	0.203

q^2 : Leave one out (LOO) cross-validated correlation coefficient; ONC: optimum number of components; r^2 : non cross-validated correlation coefficient; SEE: standard error of estimate; F : F-test value; r^2_{pred} : predicted correlation coefficient for test set of compounds; $r^2_{\text{m(test)}}$: external validated predictive potential of the model coefficient for test set; S , E , H , A , D : steric, electrostatic, hydrophobic, as well as hydrogen-bond acceptor and donor fields, respectively.

weakly hydrophobic and powerfully electronegative substituents on the 1'-position (alkyne) of thiophene may increase the activity.

3.3. Interactions between inhibitors and VEGFR-2 binding pocket

To determine the probable binding conformations of these inhibitors, AutoDock was used to dock all compounds into the active sites of VEGFR-2. Before docking the 1,4-dihydroindeno[1,2-c]pyrazoles derivatives into the VEGFR-2 binding site, the docking protocol was validated. AAZ was removed from the active site

and docked back into the binding pocket. The root mean square deviation (RMSD) between the predicted conformation and the observed X-ray crystallographic conformation of AAZ was 0.50 Å (Fig. 4). The small RMSD value indicated that the parameter set for the AutoDock simulation was reasonable to reproduce the X-ray structure. Therefore, the AutoDock method and the parameter set could be extended to search the binding conformations of other inhibitors.

To elucidate the interaction mechanism, compound 76, one of the most potent inhibitor among the whole dataset, was selected for more detailed analysis. The best possible interacting model of

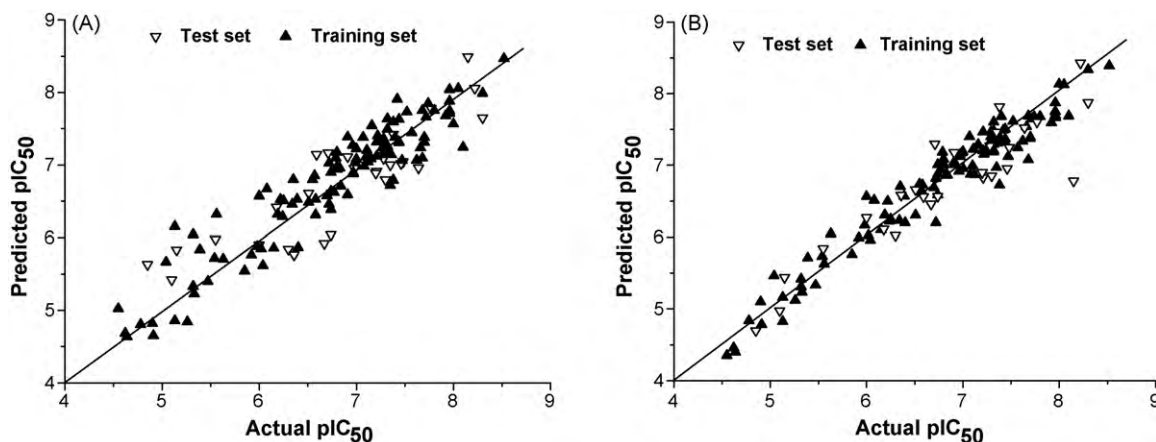


Fig. 2. Correlation between the actual and predicted activities of 3D-QSAR models (A: CoMFA model; B: CoMSIA model) for the training set and test set.

Table 3Comparison of actual and predicted pIC_{50} values of all the 140 compounds for CoMFA and CoMSIA models.

No.	pIC_{50} EA	CoMFA		CoMSIA		NO.	pIC_{50} EA	CoMFA		CoMSIA	
		PA	δ	PA	δ			PA	δ	PA	δ
1	5.92	5.764	0.156	5.987	-0.067	71	7.11	7.202	-0.092	7.227	-0.117
2	6.15	5.859	0.291	6.103	0.047	72	7.27	7.24	0.03	7.265	0.005
3	6.22	6.525	-0.305	6.499	-0.279	73	7.32	7.182	0.138	7.482	-0.162
4 [*]	4.85	5.631	-0.781	4.695	0.155	74 [*]	7.48	7.042	0.438	7.247	0.233
5	5.47	5.4	0.07	5.333	0.137	75	7.44	7.63	-0.19	7.507	-0.067
6	5.85	5.543	0.307	5.759	0.091	76	8.52	8.467	0.053	8.387	0.133
7	5.04	5.664	-0.624	5.463	-0.423	77	7.42	7.907	-0.487	7.49	-0.07
8	5.98	5.882	0.098	6.165	-0.185	78	7.96	7.71	0.25	7.696	0.264
9 [*]	6.3	5.843	0.457	6.023	0.277	79 [*]	7.35	7	0.35	7.465	-0.115
10	6.4	5.867	0.533	6.199	0.201	80	5.33	5.227	0.103	5.236	0.094
11	6.74	6.637	0.103	6.589	0.151	81	7.96	7.748	0.212	7.665	0.295
12	5.13	4.859	0.271	4.825	0.305	82	7.16	7.543	-0.383	7.288	-0.128
13	4.78	4.805	-0.025	4.838	-0.058	83	7.96	8.039	-0.079	7.752	0.208
14 [*]	5.55	5.98	-0.43	5.842	-0.292	84 [*]	8.3	7.65	0.65	7.875	0.425
15	5.26	4.841	0.419	5.119	0.141	85	8.05	8.053	-0.003	8.128	-0.078
16	4.9	4.819	0.081	5.1	-0.2	86	7.96	7.88	0.08	7.872	0.088
17	6.84	6.71	0.13	6.86	-0.02	87	7.36	7.142	0.218	7.31	0.05
18	6.08	6.67	-0.59	6.512	-0.432	88	7.62	7.066	0.554	7.339	0.281
19 [*]	6	5.904	0.096	6.269	-0.269	89 [*]	8.15	8.492	-0.342	6.78	1.37
20	6.72	6.458	0.262	6.202	0.518	90	7.4	7.381	0.019	7.683	-0.283
21	5.39	5.836	-0.446	5.711	-0.321	91	7.38	7.593	-0.213	7.392	-0.012
22	6.72	7.026	-0.306	6.818	-0.098	92	7.7	7.313	0.387	7.392	0.308
23	6.97	6.895	0.075	7.112	-0.142	93	6.91	7.385	-0.475	7.046	-0.136
24 [*]	6.18	6.416	-0.236	6.107	0.073	94 [*]	6.71	7.166	-0.456	7.298	-0.588
25	6.83	6.96	-0.13	6.876	-0.046	95	7.21	7.317	-0.107	7.203	0.007
26	7.21	7.122	0.088	7.468	-0.258	96	7.08	6.981	0.099	6.876	0.204
27	7.32	7.638	-0.318	7.605	-0.285	97	7.28	7.363	-0.083	7.232	0.048
28	6.99	7.035	-0.045	7.172	-0.182	98	7.52	7.731	-0.211	7.612	-0.092
29 [*]	6.74	6.041	0.699	6.566	0.174	99 [*]	5.1	5.424	-0.324	4.974	0.126
30	4.91	4.65	0.26	4.782	0.128	100	7.32	7.493	-0.173	7.292	0.028
31	5.56	6.321	-0.761	5.629	-0.069	101	8.3	7.989	0.311	8.335	-0.035
32	4.64	4.636	0.004	4.395	0.245	102	6.8	6.977	-0.177	7.008	-0.208
33	4.62	4.686	-0.066	4.458	0.162	103	7.32	7.257	0.063	7.21	0.11
34 [*]	6.67	5.923	0.747	6.456	0.214	104 [*]	7.21	6.914	0.296	6.828	0.382
35	7.38	6.791	0.589	6.727	0.653	105	7.29	7.27	0.02	7.467	-0.177
36	6.34	6.46	-0.12	6.233	0.107	106	6.35	6.798	-0.448	6.704	-0.354
37	5.32	5.334	-0.014	5.31	0.01	107	5.54	5.718	-0.178	5.734	-0.194
38	4.55	5.024	-0.474	4.352	0.198	108	7.47	7.063	0.407	7.121	0.349
39 [*]	5.15	5.834	-0.684	5.44	-0.29	109 [*]	6.51	6.611	-0.101	6.66	-0.15
40	6.24	6.289	-0.049	6.222	0.018	110	6.55	6.796	-0.246	6.736	-0.186
41	6.39	6.526	-0.136	6.568	-0.178	111	6.7	6.577	0.123	6.69	0.01
42	6.25	6.507	-0.257	6.25	0	112	7.1	7.113	-0.013	6.994	0.106
43	7.15	7.088	0.062	7.276	-0.126	113	6.8	6.938	-0.138	7.016	-0.216
44 [*]	6.36	5.765	0.595	6.582	-0.222	114 [*]	7.2	6.885	0.315	6.896	0.304
45	6.19	6.321	-0.131	6.309	-0.119	115	5.32	6.044	-0.724	5.417	-0.097
46	6.51	6.487	0.023	6.304	0.206	116	5.13	6.154	-1.024	5.163	-0.033
47	6.96	7.272	-0.312	6.918	0.042	117	6.74	6.386	0.354	6.875	-0.135
48	7.22	7.403	-0.183	7.153	0.067	118	7.7	7.38	0.32	7.378	0.322
49 [*]	7.3	6.796	0.504	6.852	0.448	119 [*]	6.91	7.113	-0.203	7.174	-0.264
50	7	7.224	-0.224	6.959	0.041	120	7.57	7.446	0.124	7.246	0.324
51	6.04	5.617	0.423	5.957	0.083	121	7.35	6.721	0.629	6.971	0.379
52	6.57	6.853	-0.283	6.631	-0.061	122	6.91	6.589	0.321	7.013	-0.103
53	7.44	7.318	0.122	7.37	0.07	123	7.68	7.095	0.585	7.076	0.604
54 [*]	7.28	7.087	0.193	7.27	0.01	124 [*]	7.46	7.019	0.441	6.954	0.506
55	6.58	6.314	0.266	6.618	-0.038	125	6.79	7.096	-0.306	7.184	-0.394
56	8	7.566	0.434	8.132	-0.132	126	6.58	6.526	0.054	6.725	-0.145
57	7.66	7.237	0.423	7.54	0.12	127	6.77	6.623	0.147	6.939	-0.169
58	7.3	7.229	0.071	7.353	-0.053	128	6.74	6.898	-0.158	7.01	-0.27
59 [*]	8.22	8.053	0.167	8.426	-0.206	129 [*]	6.59	7.145	-0.555	6.559	0.031
60	6.97	6.88	0.09	7.15	-0.18	130	6.8	7.174	-0.374	7.088	-0.288
61	6.02	5.848	0.172	6.024	-0.004	131	7.32	7.239	0.081	7.186	0.134
62	6	6.571	-0.571	6.562	-0.562	132	7.29	7.144	0.146	7.4	-0.11
63	7.12	7.044	0.076	6.873	0.247	133	7.96	7.727	0.233	7.68	0.28
64 [*]	7.38	7.422	-0.042	7.819	-0.439	134 [*]	6.98	6.95	0.03	7.044	-0.064
65	8.1	7.245	0.855	7.69	0.41	135	7.92	7.677	0.243	7.593	0.327
66	5.63	5.708	-0.078	6.048	-0.418	136	7.8	7.75	0.05	7.681	0.119
67	7.07	7.38	-0.31	7.399	-0.329	137	7.74	7.848	-0.108	7.679	0.061
68	7	7.079	-0.079	7.188	-0.188	138	7.72	7.662	0.058	7.651	0.069
69 [*]	7.64	6.958	0.682	7.523	0.117	139 [*]	7.77	7.779	-0.009	7.606	0.164
70	7.44	7.308	0.132	7.325	0.115	140	7.68	7.75	-0.07	7.688	-0.008

^{*} Compounds of the testing set; EA, actual pIC_{50} values; PA, predicted pIC_{50} values for CoMFA/CoMSIA model; δ , residues between actual and predicted pIC_{50} values for CoMFA/CoMSIA model.

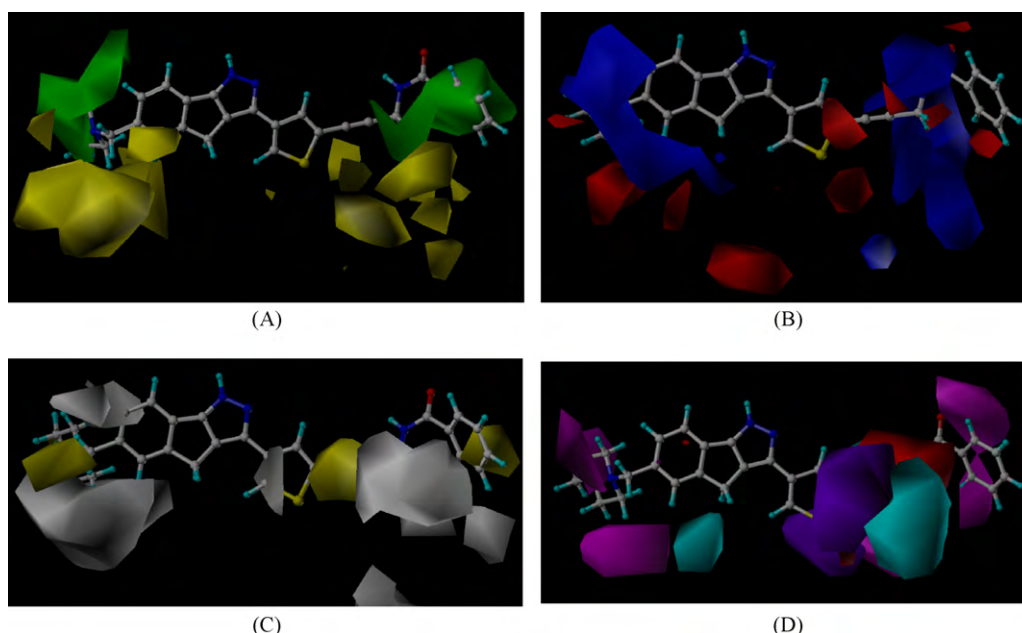


Fig. 3. CoMFA (A and B) and CoMSIA (C and D) contour maps. Sterically favored areas in green. Sterically unfavored areas in yellow. Positive-charge-favored areas in blue. Positive-charge-unfavored areas in red. Hydrophobic favored areas in yellow. Hydrophobic unfavored areas in white. Donor-favored areas in cyan. Hydrogen donor-unfavored areas in purple. Hydrogen acceptor-favored areas in magenta. Acceptor-unfavored areas in red. Compound 76 was superposed as the reference molecules in the maps. The maps generated depict regions having scaled coefficients greater than 80% (favored) or less than 20% (disfavored). (For interpretation of the references to color in this figure legend, the reader is referred to the web version of the article.)

compound 76 with VEGFR-2 and the main residues involved in the interaction were generally depicted in Fig. 5. Compound 76 was docked into the ATP binding site in such a way that its N(1)–H acts as a hydrogen-bond donor to Glu 915 and its N(2) acts as a hydrogen-bond acceptor to Cys917 in the hinge region of VEGFR-2. The 5,6-position 4'-methylpiperazine occupies a hydrophobic groove and makes significant van der Waals contacts with the hydrophobic surface of the cleft: Val846, Lys866, Arg840, Cys1043, and Phe1045. In addition, we proposed that a small hydrophobic substituent in the 5,6-position off the 4'-methylpiperazine ring would be beneficial because it would project into a small hydrophobic groove. The 3-position substituent (2',4'-linked thiophene) would provide an acceptable trajectory for the imide side chain to access the solvent. In addition, the imide group, which linked between the alkyne and the phenyl ring, formed a hydrogen-bond to the side chain of Asn921.

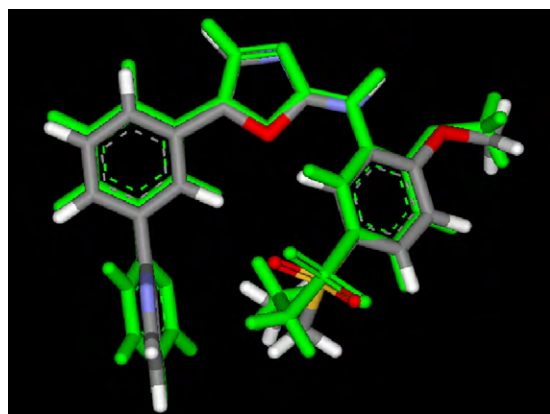
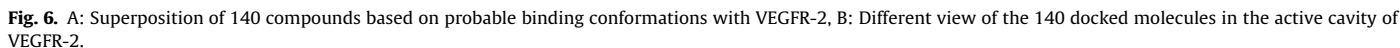
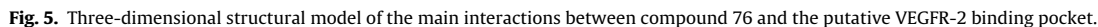


Fig. 4. Conformational comparison of AAZ from the crystal structure (by atom type color) and that from the autodock4.0 result (green). (For interpretation of the references to color in this figure legend, the reader is referred to the web version of the article.)

In our models, when the alkyne linked thiophene on 3-position was replaced by imide, NHCONH- , NHCOO- , or NHSO_2- , the groups ($=\text{O}$) (compound 102–140) could interact with the -NH or -NH_2 group of the side chain of Asn921 by forming a hydrogen-bond. The Dock approach was able to dock all of the 140 compounds into the active site with a similar pose. The docked poses of all compounds using this method are shown in Fig. 6. The docked poses serve as a very good starting point for carrying out 3D-QSAR modeling. As discussed earlier, the alignment of compound structures plays a key role in developing successful 3D-QSAR models. Hence, the docked poses of the ligands were used to develop receptor-based 3D-QSAR models.

To understand whether the pharmacological properties of the ligands are related to their electrostatic interactions with receptors, we analyzed the distribution of atomic charges on the ligand surface (Fig. 7). The potential was mapped to the solvent accessible surface, calculated with a rolling probe of radius 1.4 Å. On the surface, the red to blue colors correspond to potential values ranging from -0.100 to $+0.100$ kT/e. Comparison of electrostatic surfaces for the compound 76 (A) and the compound 76 (B) indicates that there is some correlation between the atomic charges of diverse conformation compounds and their biological activity. The 1-position nitrogen (N(1)–H) with increasingly negative and the 2-position nitrogen (N(2)), the oxygen of the imide with increasingly positive have distinct changes of charge distribution on the ligand and through the hydrogen-bond interaction of ligand and acceptor. However, the blue on the thiophene sulfur of the compound 76(B) became dense which may attribute to the interactions between the thiophene and the functional groups with carbonyl of Leu838, Phe919, Lys918, and the π -electron clouds of benzene rings of Phe916 around the thiophene. Antagonism of 4'-methylpiperazine-containing compound 76 at VEGFR-2 active site may be attributed to a combination of hydrophobicity and van der Waals interactions with surrounding receptor atoms from the putative hydrophobic ligand binding pocket.

The mechanism of antagonism of 1,4-dihydroindeno[1,2-c]pyrazoles analogues at VEGFR-2 proposed here conforms to the



molecular docking modeling, which previously explain the antagonism of 1,4-dihydroindeno[1,2-*c*]pyrazoles analogues at VEGFR-2 active site.

3.4. Docking-based 3D-QSAR models

In addition to the ligand-based 3D-QSAR, we also carried out molecular docking to understand the nature of interactions of these compounds with VEGFR-2 and receptor-based 3D-QSAR modeling, using the docked conformations of the 140 compounds in the VEGFR-2 active site. The contour plots from the receptor-based 3D-QSAR models directly relate the favorable and unfavorable contours to the corresponding detailed protein–ligand interactions in the active site.

The CoMFA and CoMSIA studies based on the flexible docking alignment by above method were conducted. The major objective of CoMFA analysis for VEGFR-2 inhibitors is to find the best predictive model within the system. PLS analysis results based on least squares fit are listed in Table 4, which shows that all of the statistical indexes are reasonably high. As listed in Table 4, CoMFA models with cross-validated q^2 of 0.563 for eight components were obtained based on the binding conformations and their alignment in the active site of VEGFR-2. The non cross-validated PLS analysis was repeated with the optimum number of components, as determined by the cross-validated analysis, to give an r^2 of 0.958, $F=291.950$, and the estimated standard error of 0.112. In addition, statistic parameter, $r^2_{m(test)} = 0.820$, indicated that the predicted activity coincided with the observed activity values for the test set

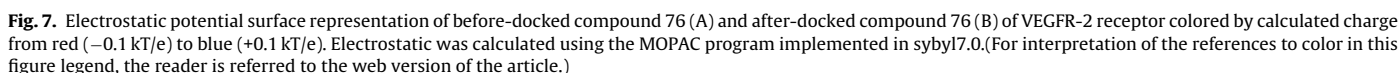


Table 4

Statistical parameters basing on docking of CoMFA and CoMSIA models of the training sets.

	ONC	q^2	r^2	SEE	F	r^2_{pred}	$r^2_{m(\text{test})}$	Field contribution				
								S	E	H	D	A
CoMFA	8	0.563	0.958	0.112	291.950	0.902	0.820	0.436	0.564			
CoMSIA	5	0.567	0.965	0.176	235.253	0.872	0.644	0.248	0.145	0.130	0.250	0.227

q^2 : Leave one out (LOO) cross-validated correlation coefficient; ONC: optimum number of components; r^2 : non cross-validated correlation coefficient; SEE: standard error of estimate; F : F-test value; r^2_{pred} : predicted correlation coefficient for test set of compounds; $r^2_{m(\text{test})}$: external validated predictive potential of the model coefficient for test set; S, E, H, A, D : steric, electrostatic, hydrophobic, as well as hydrogen-bond acceptor and donor fields, respectively.

compounds and that was a reasonable model with good external predictability. The steric and electrostatic contributions were found to be 43.6% and 56.4%, respectively. The values indicated a good conventional statistical correlation, and the CoMFA model had a fair predictive ability. The observed and calculated (predicted) activity values of these 112 compounds for CoMFA and CoMSIA and the 28 test compounds are given in Table 5. The plots of observed versus calculated activity values of training set and test set molecules for CoMFA and CoMSIA analyses are shown in Fig. 8A., indicating that the fitting power is rational and potent and the predictive ability is satisfactory.

CoMSIA analysis results are also summarized in Table 4. A CoMSIA model with q^2 value of 0.567 for five components and a conventional r^2 of 0.965, $F=235.253$, and the estimated standard error of 0.176 for inhibitors was obtained. In addition, statistic parameter for external validation, $r^2_{m(\text{test})}=0.644$, suggested that the predicted activity coincided with the observed activity values for the test set compounds. These data demonstrate that the CoMSIA model is also fairly predictive, and the predicted VEGFR-2 inhibitors potencies of these 112 compounds are listed in Table 5 and also shown in Fig. 8B. The high value of the conventional r^2 relating to five different descriptor variables (steric, electrostatic, hydrophobic, hydrogen donor and acceptor) illustrate that these variables are necessary to describe the interaction mode of inhibitors with the VEGFR-2 receptor, as well as the field properties around the inhibitors. CoMSIA analysis revealed that the steric, electrostatic, hydrophobic, hydrogen donor and acceptor field distributions are 24.8%, 14.5%, 13.0%, 25.0% and 22.7%, respectively, indicating that hydrogen-bond interactions equally dominate the binding between inhibitors and VEGFR-2.

To validate our 3D-QSAR models, 28 inhibitors (*-denoted in Table 5) that were not included in generating CoMFA and CoMSIA models were selected as testing compounds. The results are simultaneously shown in Table 5 (star labeled), Fig. 8 (in ∇ symbols). The predicted activities values are in good agreement with the experimental data in a statistically tolerable error range, $r^2_{\text{pred}}=0.902$ and

0.872 for CoMFA and CoMSIA models, respectively. In both models, the deviations of the predicted pIC_{50} values from the corresponding experimental pIC_{50} values are always smaller than 1.0 log unit. To investigate the structural differences of binding modes between the test set of compounds and the training set, automated molecular docking was performed for the test set using the same method as that of the training set. The testing results for the 28 antagonists indicate that the CoMFA and CoMSIA models can be further used in new inhibitors design for VEGFR-2.

3.5. Mapping of CoMFA and CoMSIA model onto VEGFR-2 binding site

The fields basing on ligands may hardly explain the interactions between the inhibitor and the receptor. However, we could acquire enough information for modification of the reported inhibitors and the result of our docking studies, through which can be complements of 3D-QSAR studies for drug design.

The CoMFA steric and electrostatic fields for the analysis based on the alignments of the binding conformations are presented as contour plots in Fig. 9. To aid in visualization, compound 76 is displayed in the maps. The green contour region between terminal phenyl ring and imide group shows that substituents at this position have favorable steric interactions. A small green contour beside 6-position shows that appropriately increased bulky substituents in the position will improve the biological activities (Fig. 9A). For example, compounds with the increased bulky substituents (compare 63 with 65, and 51 with 56) exhibited a considerable gain in binding affinity. Two yellow polyhedrons around the alkyne and the methylene linked the alkyne may be restricted by the Gly920, Asn921, Thr924 in steric. One near 4'-methylpiperazine group on the 6-position suggests that decreased bulky substituents in the position will improve the biological activities (Fig. 9A). For example, compounds (compare 30–36 with 70–79) significantly improve the biological activities for the decreased bulky substituents on the alkyne and the methylene.

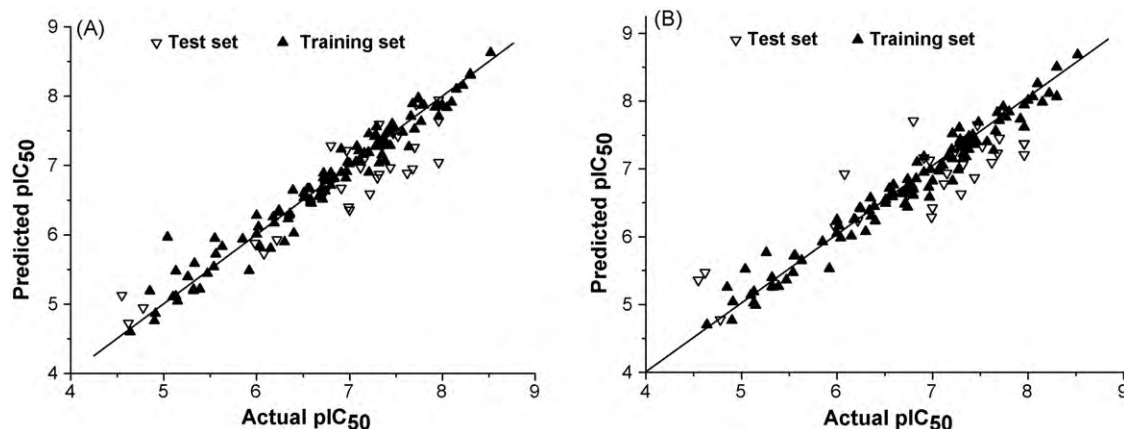


Fig. 8. Correlation between the actual and predicted activities of 3D-QSAR models (A: CoMFA model; B: CoMSIA model) for the training set and test set.

Table 5Comparison of actual and predicted pIC_{50} values of all the 140 compounds for CoMFA and CoMSIA models.

No.	pIC_{50} EA	CoMFA		CoMSIA		No.	pIC_{50} EA	CoMFA		CoMSIA	
		PA	δ	PA	δ			PA	δ	PA	δ
1	5.92	5.481	0.439	5.53	0.39	71	7.11	7.083	0.027	7.05	0.06
2	4.85	5.19	−0.34	5.253	−0.403	72	7.48	7.551	−0.071	7.688	−0.208
3	6.15	5.806	0.344	6.01	0.14	73	7.27	7.416	−0.146	6.986	0.284
4 [*]	6.22	5.93	0.29	6.24	−0.02	74 [*]	7.32	7.597	−0.277	7.427	−0.107
5	5.47	5.444	0.026	5.361	0.109	75	7.44	7.463	−0.023	7.446	−0.006
6	5.85	5.936	−0.086	5.927	−0.077	76	8.52	8.627	−0.107	8.683	−0.163
7	6.3	5.899	0.401	6.075	0.225	77	7.35	7.351	−0.001	7.422	−0.072
8	5.04	5.964	−0.924	5.522	−0.482	78	7.42	7.498	−0.078	7.503	−0.083
9 [*]	5.98	5.881	0.099	6.142	−0.162	79 [*]	7.96	7.947	0.013	7.208	0.752
10	6.4	6.024	0.376	6.231	0.169	80	5.33	5.585	−0.255	5.256	0.074
11	6.74	6.782	−0.042	6.849	−0.109	81	7.96	7.858	0.102	7.946	0.014
12	5.55	5.948	−0.398	5.714	−0.164	82	8.3	8.319	−0.019	8.067	0.233
13	5.13	5.115	0.015	5.024	0.106	83	7.16	7.178	−0.018	7.177	−0.017
14 [*]	4.78	4.945	−0.165	4.775	0.005	84 [*]	7.96	7.043	0.917	7.369	0.591
15	5.26	5.395	−0.135	5.767	−0.507	85	8.05	7.834	0.216	8.066	−0.016
16	4.9	4.758	0.142	4.766	0.134	86	7.96	7.708	0.252	7.617	0.343
17	6	6.006	−0.006	6.248	−0.248	87	8.15	8.102	0.048	7.986	0.164
18	6.84	6.814	0.026	7.097	−0.257	88	7.36	7.354	0.006	7.298	0.062
19 [*]	6.08	5.73	0.35	6.926	−0.846	89 [*]	7.62	6.893	0.727	7.095	0.525
20	6.72	6.888	−0.168	6.677	0.043	90	7.4	7.473	−0.073	7.4	0
21	5.39	5.218	0.172	5.268	0.122	91	7.38	7.359	0.021	7.404	−0.024
22	6.18	6.256	−0.076	6.256	−0.076	92	6.71	6.516	0.194	6.482	0.228
23	6.72	6.825	−0.105	6.697	0.023	93	7.7	7.522	0.178	7.71	−0.01
24 [*]	6.97	7.217	−0.247	7.127	−0.157	94 [*]	6.91	6.674	0.236	7.165	−0.255
25	6.83	6.807	0.023	6.857	−0.027	95	7.21	7.457	−0.247	7.521	−0.311
26	7.21	7.183	0.027	7.151	0.059	96	7.08	7.275	−0.195	7.028	0.052
27	6.74	6.805	−0.065	6.677	0.063	97	5.1	5.104	−0.004	5.138	−0.038
28	7.32	7.274	0.046	7.319	0.001	98	7.28	7.275	0.005	7.371	−0.091
29 [*]	6.99	6.403	0.587	6.289	0.701	99 [*]	7.52	7.425	0.095	7.333	0.187
30	4.91	4.864	0.046	5.04	−0.13	100	7.32	7.283	0.037	7.161	0.159
31	5.56	5.72	−0.16	5.723	−0.163	101	8.3	8.299	0.001	8.503	−0.203
32	6.67	6.554	0.116	6.631	0.039	102	7.21	6.9	0.31	6.823	0.387
33	4.64	4.6	0.04	4.703	−0.063	103	6.8	6.892	−0.092	6.704	0.096
34 [*]	4.62	4.727	−0.107	5.471	−0.851	104 [*]	7.32	6.876	0.444	7.07	0.25
35	7.38	7.07	0.31	7.287	0.093	105	7.29	7.561	−0.271	7.415	−0.125
36	6.34	6.229	0.111	6.389	−0.049	106	6.35	6.281	0.069	6.569	−0.219
37	5.15	5.045	0.105	4.988	0.162	107	6.51	6.604	−0.094	6.545	−0.035
38	5.32	5.196	0.124	5.399	−0.079	108	5.54	5.539	0.001	5.471	0.069
39 [*]	4.55	5.129	−0.579	5.359	−0.809	109 [*]	7.47	7.466	0.004	7.649	−0.179
40	6.24	6.354	−0.114	6.423	−0.183	110	6.55	6.664	−0.114	6.712	−0.162
41	6.39	6.643	−0.253	6.446	−0.056	111	6.7	6.665	0.035	6.635	0.065
42	6.36	6.305	0.055	6.303	0.057	112	7.2	7.189	0.011	7.288	−0.088
43	6.25	6.328	−0.078	6.41	−0.16	113	7.1	7.211	−0.111	7.073	0.027
44 [*]	7.15	7.076	0.074	6.935	0.215	114 [*]	6.8	7.284	−0.484	7.707	−0.907
45	6.19	6.168	0.022	6.253	−0.063	115	5.32	5.216	0.104	5.265	0.055
46	6.51	6.531	−0.021	6.494	0.016	116	5.13	5.477	−0.347	5.187	−0.057
47	7.3	7.3	0	7.318	−0.018	117	6.91	6.896	0.014	6.951	−0.041
48	6.96	6.818	0.142	6.731	0.229	118	6.74	6.632	0.108	6.437	0.303
49 [*]	7.22	6.59	0.63	7.214	0.006	119 [*]	7.7	7.262	0.438	7.451	0.249
50	7	7.027	−0.027	6.824	0.176	120	7.57	7.48	0.09	7.4	0.17
51	6.04	5.822	0.218	5.981	0.059	121	7.35	7.152	0.198	7.182	0.168
52	7.28	7.416	−0.136	7.604	−0.324	122	7.46	7.599	−0.139	7.403	0.057
53	6.57	6.664	−0.094	6.607	−0.037	123	6.91	7.235	−0.325	7.181	−0.271
54 [*]	7.44	6.97	0.47	6.872	0.568	124 [*]	7.68	6.954	0.726	7.233	0.447
55	6.58	6.51	0.07	6.666	−0.086	125	6.79	6.792	−0.002	6.745	0.045
56	8	7.872	0.128	8.011	−0.011	126	6.58	6.47	0.11	6.592	−0.012
57	8.22	8.155	0.065	8.117	0.103	127	6.59	6.453	0.137	6.764	−0.174
58	7.66	7.709	−0.049	7.557	0.103	128	6.77	6.812	−0.042	6.728	0.042
59 [*]	7.3	6.824	0.476	6.63	0.67	129 [*]	6.74	6.637	0.103	6.618	0.122
60	6.97	6.912	0.058	6.581	0.389	130	6.8	6.713	0.087	6.614	0.186
61	6.02	6.113	−0.093	6.161	−0.141	131	7.32	7.034	0.286	7.221	0.099
62	7.38	7.288	0.092	7.482	−0.102	132	6.98	7.046	−0.066	6.993	−0.013
63	6	6.281	−0.281	6.051	−0.051	133	7.29	7.426	−0.136	7.43	−0.14
64 [*]	7.12	6.969	0.151	6.78	0.34	134 [*]	7.96	7.643	0.317	7.376	0.584
65	8.1	7.913	0.187	8.261	−0.161	135	7.92	7.838	0.082	7.735	0.185
66	5.63	5.827	−0.197	5.652	−0.022	136	7.8	7.866	−0.066	7.84	−0.04
67	7.64	7.267	0.373	7.271	0.369	137	7.77	7.632	0.138	7.762	0.008
68	7.07	7.051	0.019	6.972	0.098	138	7.74	7.975	−0.235	7.917	−0.177
69 [*]	7	6.358	0.642	6.425	0.575	139 [*]	7.72	7.879	−0.159	7.865	−0.145
70	7.44	7.288	0.152	7.363	0.077	140	7.68	7.891	−0.211	7.831	−0.151

^{*} Compounds of the testing set; EA: actual pIC_{50} values; PA: predicted pIC_{50} values for CoMFA/CoMSIA model; δ : residues between actual and predicted pIC_{50} values for CoMFA/CoMSIA model.

One big region of blue contour near the imide group, which approach the electronegative amino acid (e.g. Thr924, Asn921), indicates that positively charged substituents may increase the antagonist activity (Fig. 9B). Three red contours around the alkyne substituent suggest that more negatively charged substituents in those positions will significantly improve the biological activities (Fig. 9B). Some electropositive amino acids, such as Phe919, Gly920, and Leu1033, distributed at those red contours validate that electronegative substituents may increase the antagonist activity.

The hydrophobic analysis of CoMSIA, based on the atomic hydrophobicity distribution, could demonstrate more clearly the hydrophobic interactions between the inhibitors and VEGFR-2. As shown in Fig. 9C, three regions of yellow contours, two around the 4'-methylpiperazine ring and the alkyne substituent and the third one near one side of the terminal phenyl ring linked the imide, indicate that adding hydrophobic substituents may increase the antagonist activity and these structural moieties interact with the side chains of residues (e.g. Lys866, Tyr925, Asn921) at the binding sites of VEGFR-2 through hydrophobic interaction. While several white-colored polyhedrons beside the imide substituent, 3'-thiophene substituent, 5-position, and on the 6-, 7-position of the 1,4-dihydroindeno[1,2-c]pyrazole framework illustrates that adding hydrophobic group at this position would be detrimental to antagonist activity. This information farther validate that small-bulk, electron-rich and hydrophilic substitutions at the alkyne substituent will increase activity.

Two regions of cyan contours near the 5-position and the methylene spacer between the alkyne and the imide group indicate that hydrogen-bond donor substituents may increase the antagonist activity (Fig. 9D). A series of amino acid, such as the Asn921 and Cys1043 with N, O, S atoms, around the methylene and the 5-position can form hydrogen-bond with the inhibitors, which indicates that hydrogen-bond donor substituents may increase

the antagonist activity. Two purple contours near the alkyne substituent and one side of the terminal phenyl ring linked the imide which forms hydrogen-bond with the amino acid Gly920 indicate that hydrogen-bond donor substituents may decrease the antagonist activity. A big magenta contour near the methylene linked the alkyne suggests that hydrogen-bond acceptor substituents may improve the biological activities and these structural moieties interact with the Thr924 at the binding sites of VEGFR-2 through hydrogen-bond interaction (Fig. 9D). The region of red contours near the imide group indicates that hydrogen-bond acceptor substituents may decrease the antagonist activity. In addition, as hydrogen-bond donor, Gly920, Asn921 and Thr924 with –OH and –NH may commendably form hydrogen-bond with the acyl group with carbonyl O atoms.

Combining the CoMFA and CoMSIA contour maps with the 3D structural topology of the VEGFR-2 binding site, several insights into the binding of inhibitors with VEGFR-2 can be readily observed. Not only does the field property coincide perfectly with the environmental characteristics of the binding pocket but also indication for some further structural modification of this kind of compounds could be found. Compounds with suitable bulky, strongly hydrophobic and weakly electronegative substituents on the 5-, 6-, 7- of framework, and with small bulky, powerfully electronegative, weakly hydrophobic substituents on the 1'-position (alkyne and methylene) of thiophene may greatly increase the activity. For example, triazole, or 4'-methylpiperazine ring systems on the 5-, 6-, 7-position are more propitious to improve their activity (e.g.: potent compound 65, 82, 101); groups (thiophene, alkyne, imide or O) are in favor of increasing the activity (e.g.: potent compound 56, 57, 65, 76, 82, 85, 87). Furthermore, as with the strongly hydrophobic 4'-methylpiperazine substituent and small bulky, electronegative alkyne (2',4'- or a 2',5'-linked thiophene on 3-position) substituent, inhibitor molecules are propitious to

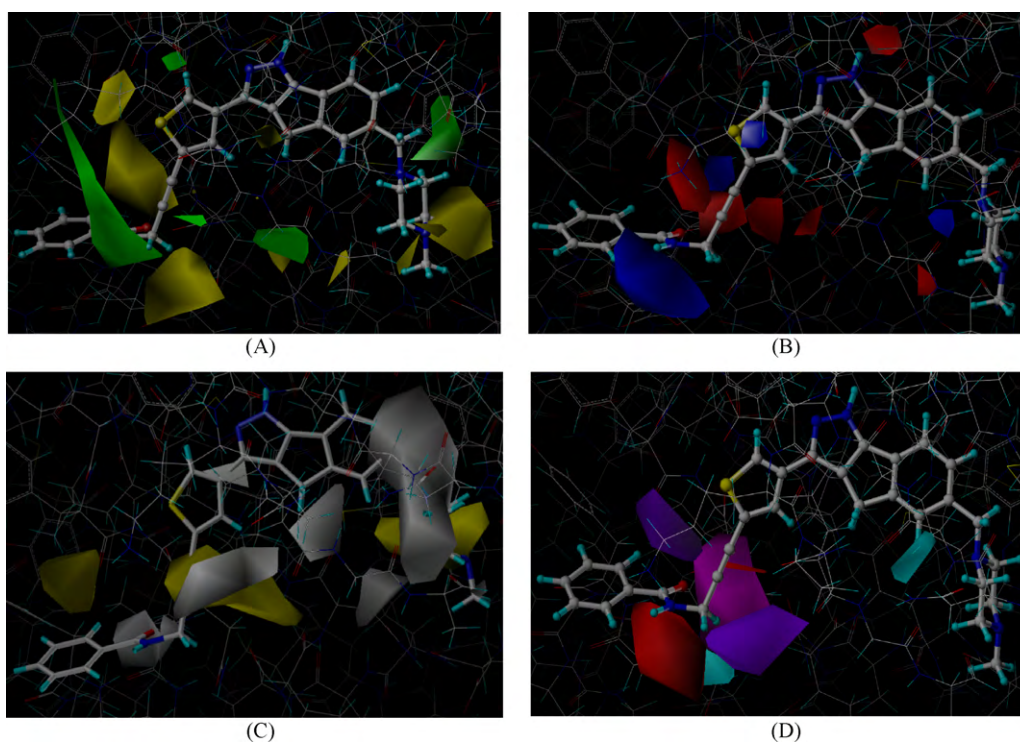


Fig. 9. CoMFA (A and B) and CoMSIA (C and D) contour maps. Sterically favored areas in green. Sterically unfavored areas in yellow. Positive-charge-favored areas in blue. Positive-charge-unfavored areas in red. Hydrophobic favored areas in yellow. Hydrophobic unfavored areas in white. Donor-favored areas in cyan. Hydrogen donor-unfavored areas in purple. Hydrogen acceptor-favored areas in magenta. Acceptor-unfavored areas in red. Compound 76 was superposed as the reference molecules in the maps. The maps generated depict regions having scaled coefficients greater than 80% (favored) or less than 20% (disfavored). (For interpretation of the references to color in this figure legend, the reader is referred to the web version of the article.)

increase the activity, it decides the structure model with 1,4-dihydroindeno[1,2-c]pyrazole as basic framework.

4. Conclusions

In this study, molecular docking and 3D-QSAR studies were carried out not only to explore the interaction mechanism between 140 inhibitors and VEGFR-2, but also to construct highly accurate and predictive 3D-QSAR models, including the CoMFA (r^2 , 0.958; q^2 , 0.563) and CoMSIA (r^2 , 0.965; q^2 , 0.567) models based on flexible docking alignment, for predicting the biological activity of new compounds. Molecular docking reveals the detailed structures of VEGFR-2 binding with the compounds. The interactions identified from the CoMFA and CoMSIA 3D contour maps correlate well with the specific interactions between the inhibitors and the amino acid residues identified in the docked binding structures. The 3D contour maps obtained from the CoMFA and CoMSIA models in combination with the detailed VEGFR-2 inhibitor binding structures obtained from molecular docking help to better interpret the structure–activity relationship of these VEGFR-2 inhibitors and provide valuable insights into rational drug design for further improvement of the biological activity of the VEGFR-2 inhibitors.

Acknowledgements

The authors are gratefully acknowledged financial support from the Natural Science Foundation of China (NO.: 20671013).

References

- [1] D. Jurgen, H.A. Daniel, D.A. Lee, K.L. Ashworth, A.Z. Irini, P.F. Bousquet, J.J. Bouska, G.A. Cunha, S.K. Davidsen, G.J. Diaz, S.W. Djuric, A.F. Gasiecki, G.A. Gintant, V.J. Gracias, C.M. Harris, K.A. Houseman, C.W. Hutchins, E.F. Johnson, H. Li, P.A. Marcotte, R.L. Martin, M.R. Michaelides, M. Nyein, T.J. Sowin, Z. Su, P.H. Tapang, Z. Xia, H.Q. Zhang, 1,4-dihydroindeno[1,2-c]pyrazoles with acetylenic side chains as novel and potent multitargeted receptor tyrosine kinase inhibitors with low affinity for the hERG ion channel, *J. Med. Chem.* 50 (2007) 2011–2029.
- [2] D.R. Robinson, Y.M. Wu, S.F. Lin, The protein tyrosine kinase family of the human genome, *Oncogene* 19 (2000) 5548–5557.
- [3] A. Ullrich, J. Schlessinger, Signal transduction by receptors with tyrosine kinase activity, *Cell* 61 (1990) 203–212.
- [4] D. Rousset, F. Agnes, P. Lachau, C. Andre, F. Galibert, Molecular evolution of the genes encoding receptor tyrosine kinase with immunoglobulinlike domains, *J. Mol. Evol.* 41 (1995) 421–429.
- [5] O. Potapova, A.D. Laird, M.A. Nannini, A. Barone, G. Li, K.G. Moss, J.M. Cherrington, D.B. Mendel, Contribution of individual targets to the antitumor efficacy of the multitargeted receptor tyrosine kinase inhibitor SU11248, *Mol. Cancer Ther.* 5 (2006) 1280–1289.
- [6] G. Ranieri, R. Patrino, E. Ruggieri, S. Montemurro, P. Valerio, D. Ribatti, Vascular endothelial growth factor (VEGF) as a target of Bevacizumab in Cancer: from the biology to the clinic, *Curr. Med. Chem.* 13 (2006) 1845–1857.
- [7] C. Uchida, T.L. Haas, Evolving strategies in manipulating VEGF/VEGFR signaling for the promotion of angiogenesis in ischemic muscle, *Curr. Pharm. Des.* 15 (2009) 411–421.
- [8] G.A. Fava, Affective disorders and endocrine disease. New insights from psychosomatic studies, *Psychosomatics* 35 (1994) 341–353.
- [9] D.A. Walsh, L. Haywood, Angiogenesis: a therapeutic target in arthritis, *Curr. Opin. Invest. Drug.* 2 (2001) 1054–1063.
- [10] L.P. Aiello, R.L. Avery, P.G. Arrigg, B.A. Key, H.D. Jampel, S.T. Shah, L.R. Pasquale, H. Thieme, M.A. Iwamoto, J.E. Park, H.V. Nguyen, L.M. Aiello, N. Ferrara, G.L. King, Vascular endothelial growth factor in ocular fluid of patients with diabetic retinopathy and other retinal disorders, *N. Engl. J. Med.* 331 (1994) 1480–1487.
- [11] M. Detmar, The role of VEGF and thrombospondins in skin angiogenesis, *J. Dermatol. Sci.* 24 (2000) 78–84.
- [12] J. Folkman, Anti-angiogenesis: new concept for therapy of solid tumors, *Ann. Surg.* 175 (1972) 409–416.
- [13] L.A. Liotta, P.S. Steeg, W.G. Stetler-Stevenson, Cancer metastasis and angiogenesis: an imbalance of positive and negative regulation, *Cell* 64 (1991) 327–336.
- [14] L.C. Ewan, H.M. Jopling, H. Jia, S. Mittar, A. Bagherzadeh, G.J. Howell, J. Gareth, J.H. Walker, I.C. Zachary, S. Ponnambalam, Intrinsic tyrosine kinase activity is required for vascular endothelial growth factor receptor 2 ubiquitination, sorting and degradation in endothelial cells, *Traffic* 7 (2006) 1270–1282.
- [15] M. Dougher, B.I. Terman, Autophosphorylation of KDR in the kinase domain is required for maximal VEGF-stimulated kinase activity and receptor internalization, *Oncogene* 18 (1999) 1619–1627.
- [16] M.G. Lampugnani, F. Orsenigo, M.C. Gagliani, C. Tacchetti, E. Dejana, Vascular endothelial cadherin controls VEGFR-2 internalization and signaling from intracellular compartments, *J. Cell. Biol.* 174 (2006) 593–604.
- [17] N. Ferrara, VEGF and the quest for tumour angiogenesis factors, *Nat. Rev. Cancer* 2 (2002) 795–803.
- [18] P. Carmeliet, R.K. Jain, Angiogenesis in cancer and other diseases, *Nature* 407 (2000) 249–257.
- [19] S. Baka, A.R. Clamp, G.C. Jayson, A review of the latest clinical compounds to inhibit VEGF in pathological angiogenesis, *Expert Opin. Ther. Targets* 10 (2006) 867–876.
- [20] B.M. Klebl, G. Muller, Second-generation kinase inhibitors, *Expert Opin. Ther. Targets* 9 (2005) 975–993.
- [21] K. Holmes, O.L. Roberts, A.M. Thomas, M.J. Cross, Vascular endothelial growth factor receptor-2: structure, function, intracellular signalling and therapeutic inhibition, *Cell Signal* 19 (2007) 2003–2012.
- [22] H. Zhong, J. Phillip Bowen, Molecular design and clinical development of VEGFR kinase inhibitors, *Curr. Top. Med. Chem.* 7 (2007) 1379–1393.
- [23] N. Ferrara, K.J. Hillan, H.P. Gerber, W. Novotny, Discovery and development of bevacizumab, an anti-VEGF antibody for treating cancer, *Nat. Rev. Drug Discov.* 3 (2004) 391–400.
- [24] B. Ruggeri, J. Singh, D. Gingrich, T. Angeles, M. Albom, S. Yang, H. Chang, C. Robinson, K. Hunter, P. Dobrzanski, S. Jones-Bolin, S. Pritchard, L. Aimone, A. Klein-Szanto, J.M. Herbert, F. Bono, P. Schaeffer, P. Casellas, B. Bourie, R. Pili, J. Isaacs, M. Ator, R. Hudkins, J. Vaught, J. Mallamo, C. Dionne, CEP-7055: a novel, orally active pan inhibitor of vascular endothelial growth factor receptor tyrosine kinases with potent antiangiogenic activity and antitumor efficacy in preclinical models, *Cancer Res.* 63 (2003) 5978–5991.
- [25] A.L. Thomas, B. Morgan, J. Dreves, C. Unger, B. Wiedenmann, U. Vanhoefer, D. Laurent, M. Dugan, W.P. Steward, Vascular endothelial growth factor receptor tyrosine kinase inhibitors: PTK787/ZK 222584, *Semin. Oncol.* 30 (2003) 32–38.
- [26] J.S. Beebe, J.P. Jani, E. Knauth, P. Goodwin, C. Higdon, A.M. Rossi, E. Emerson, M. Finkelstein, E. Floyd, S. Harriman, J. Atherton, S. Hillerman, C. Soderstrom, K. Kou, T. Gant, M.C. Noe, B. Foster, F. Rastinejad, M.A. Marx, T. Schaeffer, P.M. Whalen, W.G. Roberts, Pharmacological characterization of CP-547,632, a novel vascular endothelial growth factor receptor-2 tyrosine kinase inhibitor for cancer therapy, *Cancer Res.* 63 (2003) 7301–7309.
- [27] K.M. Sakamoto, Su-11248 Sugen, *Curr. Opin. Invest. Drug* 5 (2004) 1329–1339.
- [28] T. Ahman, T. Eisen, Kinase Inhibition with BAY 43-9006 in renal cell carcinoma, *Clin. Cancer Res.* 10 (2004) 6388–6392.
- [29] A.J. Ryan, S.R. Wedge, ZD6474-a novel inhibitor of VEGFR and EGFR tyrosine kinase activity, *Br. J. Cancer* 92 (2005) 6–13.
- [30] A. Polverino, A. Coxon, C. Starnes, Z. Diaz, T. DeMelfi, L. Wang, J. Bready, J. Estrada, R. Cattley, S. Kaufman, D. Chen, Y. Gan, G. Kumar, J. Meyer, S. Neervannan, G. Alva, J. Talvenheim, S. Montestruque, A. Tasker, V. Patel, R. Radinsky, R. Kendall, AMG 706, an oral, multitargeted inhibitor that selectively targets vascular endothelial growth factor, platelet-derived growth factor, and kit receptors, potentially inhibits angiogenesis and induces regression in tumor xenografts, *Cancer Res.* 66 (2006) 8715–8721.
- [31] A. Wissner, M.B. Floyd, B.D. Johnson, H. Fraser, C. Ingalls, T. Nittoli, R.G. Dushin, C. Discafani, R. Nilakantan, J. Marini, M. Ravi, K. Cheung, X. Tan, S. Musto, T. Annable, M.M. Siegel, F. Loganzo, 2-(Quinazolin-4-ylamino)-[1,4]benzoquinones as covalent-binding, irreversible inhibitors of the kinase domain of vascular endothelial growth factor receptor-2, *J. Med. Chem.* 48 (2005) 7560–7581.
- [32] R.S. Bhide, Z.W. Cai, Y.Z. Zhang, L. Qian, D. Wei, S. Barbosa, L.J. Lombardo, R.M. Borzilleri, X. Zheng, L.I. Wu, J.C. Barrish, S.H. Kim, K. Leavitt, A. Mathur, L. Leith, S. Chao, B. Wautlet, S. Mortillo, R. Jeyaseelan, D. Kukral, J.T. Hunt, A. Kamath, A. Fura, V. Vyas, P. Marathe, C. D'Arienzo, G. Derbin, J. Fargnoli, Discovery and preclinical studies of (R)-1-(4-(4-fluoro-2-methyl-1H-indol-5-yloxy)-5-methylpyrrolo[2,1-f][1,2,4]triazin-6-yloxy)propan-2-ol (BMS-540215), an in vivo active potent VEGFR-2 inhibitor, *J. Med. Chem.* 49 (2006) 2143–2146.
- [33] R.M. Borzilleri, R.S. Bhide, J.C. Barrish, C.J. D'Arienzo, G.M. Derbin, J. Fargnoli, J.T. Hunt, R. Jeyaseelan, A. Kamath, D.W. Kukral, P. Marathe, S. Mortillo, L. Qian, J.S. Tokarski, B.S. Wautlet, X. Zheng, L.J. Lombardo, Discovery and evaluation of N-cyclopropyl-2,4-difluoro-5-((2-(pyridin-2-ylamino)thiazol-5-ylmethyl)amino)-benzamide (BMS-605541), a selective and orally efficacious inhibitor of vascular endothelial growth factor receptor-2, *J. Med. Chem.* 49 (2006) 3766–3769.
- [34] M.H. Potashman, J. Bready, A. Coxon, T.M. DeMelfi, L. DiPietro, N. Doerr, D. Elbaum, J. Estrada, P. Gallant, J. Germain, Y. Gu, J.C. Harmange, S.A. Kaufman, R. Kendall, J.L. Kim, G.N. Kumar, A.M. Long, S. Neervannan, V.F. Patel, A. Polverino, P. Rose, S. vanderPlas, D. Whittington, R. Zanon, H. Zhao, Design, synthesis, and evaluation of orally active benzimidazoles and benzoxazoles as vascular endothelial growth factor-2 receptor tyrosine kinase inhibitors, *J. Med. Chem.* 50 (2007) 4351–4373.
- [35] M. Hasegawa, N. Nishigaki, Y. Washio, K. Kano, P.A. Harris, H. Sato, I. Mori, R.I. West, M. Shibahara, H. Toyoda, L. Wang, R.T. Nolte, J.M. Veal, M. Cheung, Discovery of novel benzimidazoles as potent inhibitors of TIE-2 and VEGFR-2 tyrosine kinase receptors, *J. Med. Chem.* 50 (2007) 4453–4470.
- [36] Z.-w. Cai, D. Wei, R.M. Borzilleri, L. Qian, A. Kamath, S. Mortillo, B. Wautlet, B.J. Henley, R. Jeyaseelan Sr., J. Tokarski, J.T. Hunt, R.S. Bhide, J. Fargnoli, L.J. Lombardo, Synthesis, SAR, and evaluation of 4-[2,4-difluoro-5-(cyclopropylcarbamoyl)phenylamino] pyrrolo[2,1-f][1,2,4]triazine-based VEGFR-2 kinase inhibitors, *Bioorg. Med. Chem. Lett.* 18 (2008) 1354–1358.
- [37] O. Ilavich, O. Jacobson, Y. Aviv, A. Litchi, R. Chisin, E. Mishani, Formation of fluorine-18 labeled diaryl ureas – labeled VEGFR-2/PDGFR dual inhibitors as

- molecular imaging agents for angiogenesis, *Bioorg. Med. Chem.* 16 (2008) 4242–4251.
- [38] R. Ruel, C. Thibeault, A. L'Heureux, A. Martel, Z.-W. Cai, D. Wei, L. Qian, J.C. Barrish, A. Mathur, C. D'Arienzo, J.T. Hunt, A. Kamath, P. Marathe, Y. Zhang, G. Derbin, B. Wautlet, S. Mortillo, R. Jeyaseelan Sr., B. Henley, R. Tejwani, R.S. Bhide, G.L. Trainor, J. Fargnoli, L.J. Lombardo, Discovery and preclinical studies of 5-isopropyl-6-(5-methyl-1,3,4-oxadiazol-2-yl)-N-(2-methyl-1H-pyrrolo[2,3-b]pyridin-5-yl)pyrrolo[2,1-f][1,2,4]triazin-4-amine (BMS-645737), an in vivo active potent VEGFR-2 inhibitor, *Bioorg. Med. Chem. Lett.* 18 (2008) 2985–2989.
- [39] I. Akritopoulou-Zanze, D.H. Albert, P.F. Bousquet, G.A. Cunha, C.M. Harris, M. Moskey, J. Dinges, K.D. Stewart, T.J. Sowin, Synthesis and biological evaluation of 5-substituted 1,4-dihydroindeno[1,2-c]pyrazoles as multitargeted receptor tyrosine kinase inhibitors, *Bioorg. Med. Chem. Lett.* 17 (2007) 3136–3140.
- [40] J. Dinges, I. Akritopoulou-Zanze, L.D. Arnold, T. Barlozzari, P.F. Bousquet, G.A. Cunha, A.M. Ericsson, N. Iwasaki, M.R. Michaelides, N. Ogawa, K.M. Phelan, P. Rafferty, T.J. Sowin, K.D. Stewart, Z. Xiaa, H.Q. Zhang, Hit-to-lead optimization of 1,4-dihydroindeno[1,2-c]pyrazoles as a novel class of KDR kinase inhibitors, *Bioorg. Med. Chem. Lett.* 16 (2006) 4371–4375.
- [41] J. Dinges, K.L. Ashworth, I. Akritopoulou-Zanze, L.D. Arnold, S.A. Baumeister, P.F. Bousquet, G.A. Cunha, S.K. Davidsen, S.W. Djuric, V.J. Gracias, M.R. Michaelides, P. Rafferty, T.J. Sowin, K.D. Stewart, Z. Xiaa, H.Q. Zhang, 1,4-Dihydroindeno[1,2-c]pyrazoles as novel multitargeted receptor tyrosine kinase inhibitors, *Bioorg. Med. Chem. Lett.* 16 (2006) 4266–4271.
- [42] Y.C. Martin, 3D-QSAR: Current state, scope, and limitations, *Perspect. Drug Disc. Des.* 12 (1998) 3–23.
- [43] R.D. Cramer, D.E. Patterson, J.D. Bunce, Comparative molecular field analysis (CoMFA). 1. Effect of shape on binding of steroids to carrier proteins, *J. Am. Chem. Soc.* 110 (1988) 5959–5967.
- [44] G. Klebe, U. Abraham, T. Mietzner, Molecular similarity indices in a comparative analysis (CoMSIA) of drug molecules to correlate and predict their biological activity, *J. Med. Chem.* 37 (1994) 4130–4146.
- [45] H. Kubinyi, Comparative molecular field analysis (CoMFA), in: P.V.R. Schleyer, N.L. Allinger, T. Clark, J. Gasteiger, P.A. Kollman, H.F. Schaefer III, P.R. Schreiner (Eds.), *The Encyclopedia of Computational Chemistry*, 1, John Wiley & Sons, Chichester, UK, 1998, pp. 448–460.
- [46] M. Bohm, J. Sturzebecher, G. Klebe, Three dimensional quantitative structure activity relationship analyses using comparative molecular field analysis and comparative molecular similarity indices analysis to elucidate selectivity differences of inhibitors binding to trypsin, thrombin, and factor Xa, *J. Med. Chem.* 42 (1999) 458–477.
- [47] A.K. Debnath, Quantitative structure-activity relationship (QSAR) paradigmsHansch era to new millennium, *Mini-Rev. Med. Chem.* 1 (2001) 187–195.
- [48] G.F. Yang, H.T. Lu, Y. Xiong, C.G. Zhan, Understanding the structure-activity and structure-selectivity correlation of cyclic guanine derivatives as phosphodiesterase-5 inhibitors by molecular docking, CoMFA and CoMSIA analyses, *Bioorg. Med. Chem.* 14 (2006) 1462–1473.
- [49] X. Huang, L. Xu, X. Luo, K. Fan, R. Ji, G. Pei, K. Chen, H. Jiang, Elucidating the inhibiting mode of AHPBA derivatives against HIV-1 protease and building predictive 3D-QSAR models, *J. Med. Chem.* 45 (2002) 333–343.
- [50] Sybyl Version 7.0, St. Louis (MO), Tripos Associates Inc., 2004, URL <http://www.tripos.com>.
- [51] M. Clark, R.D.I. Cramer, N.V. Opdenbosch, Validation of the general purpose tripos 5.2 force field, *J. Comput. Chem.* 10 (1989) 982–1012.
- [52] J. Gasteiger, M. Marsili, Iterative partial equalization of orbital electronegativity – a rapid access to atomic charges, *Tetrahedron* 36 (1980) 3219–3228.
- [53] S.J. Weiner, P.A. Kollman, D.A. Case, C. Singh, G. Ghio, S. Alagona, P. Profeta, P. Weiner, A new force field for molecular mechanical simulation of nucleic acids and proteins, *J. Am. Chem. Soc.* 106 (1984) 765–784.
- [54] J. Zeng, G. Liu, Y. Tang, H. Jiang, 3D-QSAR studies on fluoropyrrolidine amides as dipeptidyl peptidase IV inhibitors by CoMFA and CoMSIA, *J. Mol. Model* 13 (2007) 993–1000.
- [55] R.D. Cramer III, D.E. Patterson, J.D. Bunce, Comparative molecular field analysis (CoMFA). 1. Effect of shape on binding of steroids to carrier proteins, *J. Am. Chem. Soc.* 110 (1988) 5959–5967.
- [56] S. Wold, A. Ruhe, H. Wold, W.J. Dunn, The collinearity problem in linear regression. The partial least squares (PLS) approach to generalized inverses *SIAM, J. Sci. Stat. Comput.* 5 (1984) 735–743.
- [57] B.L. Bush, R.B. Nachbar, Sample-distance partial least squares: PLS optimized variables, with the application to CoMFA, *J. Comput. Aided Mol. Des.* 7 (1993) 587–619.
- [58] P.P. Roy, S. Paul, I. Mitra, K. Roy, On two novel parameters for validation of predictive QSAR models, *Molecules* 14 (2009) 1660–1701.
- [59] G.M. Morris, D.S. Goodsell, R.S. Halliday, R. Huey, W.E. Hart, R.K. Belew, A.J. Olson, Automated docking using a Lamarckian genetic algorithm and an empirical binding free energy function, *J. Comput. Chem.* 19 (1998) 1639–1662.
- [60] E.L. Mehler, T. Solmajer, Electrostatic effects in proteins: comparison of dielectric and charge models, *Protein Eng.* 4 (1991) 903–910.